Journal of Power Sources 196 (2011) 208–217

Contents lists available at ScienceDirect

Journal of Power Sources

journal homepage: www.elsevier.com/locate/jpowsour

Modeling and control of tubular solid-oxide fuel cell systems: II. Nonlinear model reduction and model predictive control

Borhan M. Sanandaji, Tyrone L. Vincent*, Andrew M. Colclasure, Robert J. Kee

Engineering Division, Colorado School of Mines, 1600 Illinois St., Golden, CO 80401, USA

ARTICLE INFO

Article history:
Received 13 May 2010
Received in revised form 18 June 2010
Accepted 21 June 2010
Available online 3 July 2010

Keywords:
Tubular SOFC
Physical modeling
Model predictive control
Nonlinear system identification
Linear parameter varying models

ABSTRACT

This paper describes a systematic method for developing model-based controllers for solid-oxide fuel cell (SOFC) systems. To enhance the system efficiency and to avoid possible damages, the system must be controlled within specific operating conditions, while satisfying a load requirement. Model predictive control (MPC) is a natural choice for control implementation. However, to implement MPC, a low-order model is needed that captures the dominant dynamic behavior over the operating range. A linear parameter varying (LPV) model structure is developed and applied to obtain a control-oriented dynamic model of the SOFC stack. This approach effectively reduces a detailed physical model to a form that is compatible with MPC. The LPV structure includes nonlinear scheduling functions that blend the dynamics of locally linear models to represent nonlinear dynamic behavior over large operating ranges. Alternative scheduling variables are evaluated, with cell current being shown to be an appropriate choice. Using the reduced-order model, an MPC controller is designed that can respond to the load requirement over a wide range of operation changes while maintaining input–output variables within specified constraints. To validate the approach, the LPV-based MPC controller is applied to the high-order physical model.

1. Introduction

This paper is the second of a two-part paper that develops a model-based approach for control of a tubular solid-oxide fuel cell (SOFC) system. The companion paper develops the physical model and applies linear model-reduction techniques near particular steady-state operating points (OPs) [1]. The present paper continues to use the same physical model, but develops linear parameter varying (LPV) methods to extend the reduced models over large ranges of operating conditions. Finally, the reduced models are used to develop and demonstrate model predictive control (MPC).

1.1. SOFC systems

Fuel cells are devices that enable the direct conversion of chemical energy into electrical energy, with a theoretical conversion efficiency that can be much higher than for heat engines [2]. As illustrated in Fig. 1, the systems are an integrated combination of contributing components including the fuel cell stack, together with balance of plant (BOP) components that include air blowers, fuel pump, fuel reformer (e.g., catalytic partial oxidation (CPOX)), tail-gas combustor, heat exchangers, power conditioning unit, etc. [3].

In a system such as the one illustrated in Fig. 1, vaporized fuel and air are converted within a CPOX reactor to produce a syngas mixture (i.e., a mixture of H_2, H_2O, CO, CO_2, and N_2). The syngas enters the anode side of the SOFC stack. Preheated air enters the cathode side of the SOFC stack. Air and unspent fuel leaving the stack are mixed and burned in a catalytic tail-gas combustor. Hot gases leaving the tail-gas burner are used in a recuperating heat exchanger to preheat the air entering the SOFC stack. Raw power from the SOFC is processed through power electronics before being delivered to the application load.

1.2. Why is a control system necessary?

To operate at multiple power levels, fuel cells require a control system to balance the fuel and air supply, as well as the electrical load. This is important both to achieve high efficiency, as well as to avoid operating conditions that can damage the fuel cell, such as excessive temperature or temperature gradients, catalyst coking, and anode reoxidation. Especially for small portable power applications, the SOFC must deliver power profiles that meet the transient load demands. Consider, for example, an auxiliary power unit (APU) that is designed to satisfy the hotel loads for the sleeper cab on a long-haul truck. Depending upon the activities and appliances in the cab, the power demanded from the APU can vary considerably

* Corresponding author. Tel.: +1 303 273 3641; fax: +1 303 273 3602.
E-mail address: tvincent@mines.edu (T.L. Vincent).

0378-7753/$ – see front matter © 2010 Elsevier B.V. All rights reserved.
doi:10.1016/j.jpowsour.2010.06.075

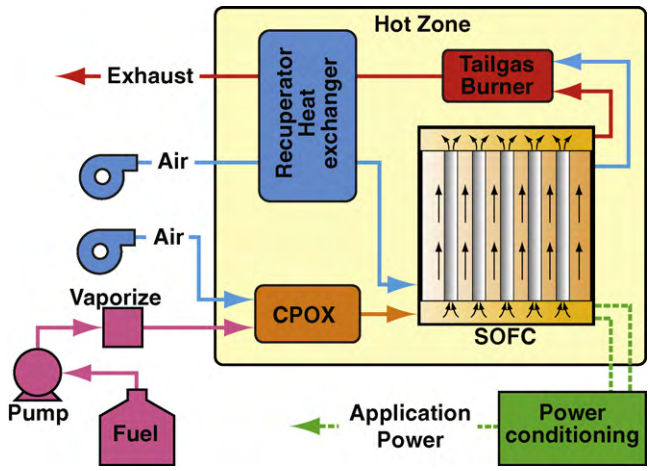

Fig. 1. Schematic of an SOFC system that is typical for mobile applications such as an APU.

over time. Although such systems are usually designed with battery storage and power electronics that seek to limit the transients required from the SOFC, the fuel-cell system must still respond to a range of transients. Moreover, if a control system can enable the fuel cell to respond to load changes more quickly, storage requirements are reduced, decreasing overall system cost.

Any control system depends upon actuation and sensing. SOFC actuation is usually accomplished through a combination of cell operating voltage, fuel flow rate, and air flow rate. Sensing is usually accomplished with thermocouples that measure temperature. Pressure and flow-rate measurements are valuable, if available. Measuring chemical composition is especially valuable but usually difficult and expensive. Thus, chemical information usually must be inferred from other less-expensive measurements. There are usually practical constraints on actuation and on system performance to avoid damage to the cell. For example, the operating voltage may be constrained to remain above 0.6 V. The cell temperature may be constrained to remain within a specified range. Fuel utilization is usually constrained such that some unspent fuel remains in the anode exhaust. A sophisticated control system is needed to meet constraints on actuation and response while guiding the system through power-demand transients [4].

1.3. Prior modeling research

For a model to be useful for control purposes, it must be of low complexity and yet capture the dominant dynamic behavior of the system. Control-oriented modeling ranges from first principles physics-based component modeling using flow characteristics, mass- and energy-balances, simple diffusion and heat equations to data-driven methods that fit low-order empirical models to experimental data.

Examples of physics-based low-order modeling include, Hall and Colclaser [5], who develop a transient model for a tubular SOFC, Padulles et al. [6], who propose an integrated SOFC plant dynamic for power systems simulation and Pukrushpan et al. [7], who develop physics-based dynamic models of proton exchange membrane fuel cell (PEMFC).

One difficulty of physics-based low-order modeling is that when choosing which physical effects to include, it is often difficult to balance between computational simplicity and physical fidelity. As an alternative, many investigators adopt a data-based approach, which begins with data from either a high-order model or an experiment and fits a low-order empirical model. For example, Yang et al. [8] consider a modified Takagi-Sugeno fuzzy (TSF) modeling and identification of an SOFC stack. Arriagada et al. [9] develop an SOFC model based on an artificial neural network (ANN). Huo et al. [10] develop a Hammerstein model consisting of a static nonlinear block followed in series by a dynamic linear block. Wang et al. [11] consider a data-driven modeling approach for identifying SOFC systems.

All the foregoing examples have limitations. In some cases, even when nonlinear model structures were used, only static (steady-state) models were considered. In other cases, transient models are used, but they are only fit near a single OP. Such modeling approaches are generally less useful for control because changes in the required load on the SOFC stack cause both the steady-state equilibrium and dynamic response to vary significantly at different OPs.

Recent research by Hasikos et al. [12] for PEMFCs considers multiple OPs. They generate a steady-state database of manipulated and controlled variables and then fit an ANN model to that database. After static modeling, dynamic behavior is added to the model by including a finite impulse response (FIR) model of the system at one of the OPs. Chen et al. [13] present a multiple-model approach for a PEMFC/ultracapacitor system. They use fuzzy clustering to characterize and identify multiple linear models of the system, which are selected based on operating conditions.

1.4. Prior control research

A variety of control approaches has been proposed for fuel cell systems, ranging from simple linear state feedback controllers to more advanced control techniques such as predictive controllers. Li et al. [14] used a state feedback exact linearization approach. Pukrushpan et al. [7] considered dynamic feedforward and state feedback controllers along with the linear quadratic (LQ) methodology.

Several authors, including, Danzer et al. [15], Yang et al. [16], Jurado [17], and Huo et al. [10] considered using MPC for fuel-cell systems. MPC uses a system model and an online optimization to calculate appropriate actuation commands. This is an attractive option for SOFC systems, because MPC can directly handle constraints on both the input and output variables. However, in most prior implementations of MPC, control is only demonstrated around one particular OP.

Hasikos et al. [12] developed an integrated optimization and control tool for PEMFC systems. After fitting a radial basis function (RBF) neural network model to a steady-state database, an MPC methodology was designed based on a FIR model of the system at one specific OP. This results in relatively poor transient response with long rise time and/or output jitter when the system is operated away from the nominal OP selected for FIR modeling. Chen et al. [13] considered a multiple-model predictive controller for a hybrid PEMFC system. In multiple-model MPC design, an upper-layer adaptive switch is added that determines which of the models should be used within each sampling period. However, the implementation can be computationally expensive and switching between linearized models can cause unintended perturbations.

1.5. The present approach

The present approach to control of the SOFC stack is to develop an MPC controller based upon reducing a complex physical model of the stack [1], with the low-complexity model being specifically tailored for real-time optimization. The model reduction is based on a specific LPV model structure that continuously blends multiple linear models according to a so-called scheduling parameter. A *velocity implementation* is used to ensure that only small-signal information is applied to the linear models, thus assuring bumpless transfer between OPs [18].

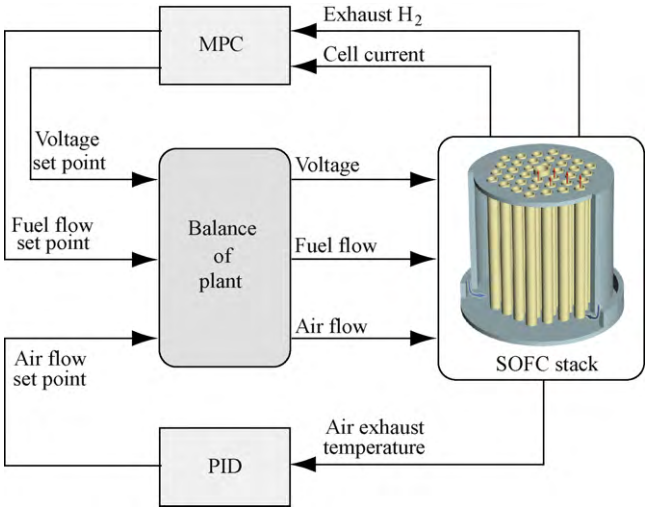

Fig. 2. System block diagram showing input–output allocation of the control structure. Note that the tubes in the SOFC stack are in a parallel configuration in regard to the fuel and air, but in a series configuration electrically, so that the stack voltage is the sum of the tube voltages.

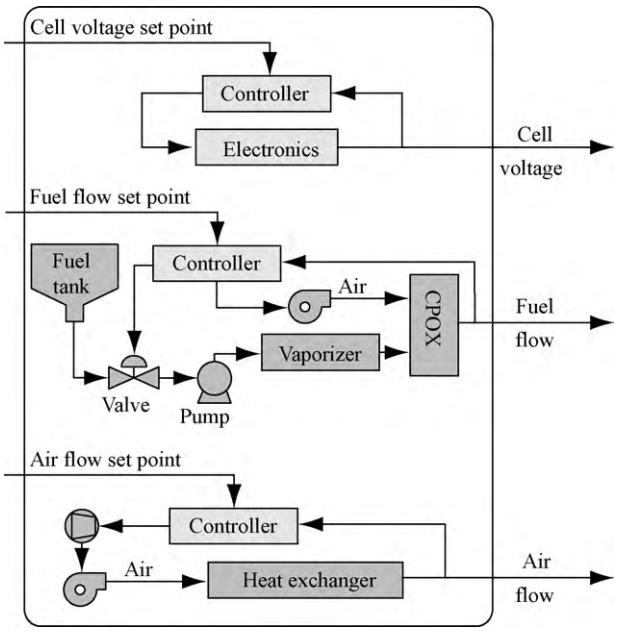

Fig. 3. Balance of plant subsystems.

Model reduction proceeds in two steps. In the first step, a set of OPs is selected. At each OP the physical model is systematically perturbed and the model response is recorded. A linear model can be identified using the relationships between perturbations and responses. As discussed in the companion paper [1], the linear models capture the small-signal behavior of the SOFC stack near the selected OPs. This linear identification is followed by a second step in which nonlinear scheduling functions are identified that modulate the outputs of the small-signal models in a manner similar to gain scheduling. A particular contribution of the present paper is a novel non-parametric approach for identifying the scheduling functions. In the LPV scheme, one of the measurable output variables is considered to be the scheduling variable. Alternative choices for scheduling parameters, and combinations of scheduling parameters, are investigated. An LPV-based MPC controller is designed, implemented, and tested. Controller performance is evaluated by controlling simulations based upon the detailed physical model while the MPC controller exploits the low-order fast model of the stack in its online calculations. Several demand trajectories are evaluated, considering rapid transients in output power while satisfying constraints on cell voltage, fuel flow rate, and fuel utilization.

2. Control strategy

As illustrated in Fig. 2, the system-level control strategy is hierarchical, with MPC used at the highest level. The SOFC system is comprised of the stack, shown on the right, and the BOP components. Fig. 3 illustrates the interior structure of the BOP block, which regulates voltage, fuel flow rate, and air flow rate. Since the tubes (cells) in the stack are connected electrically in series, the regulated voltage is the sum of the individual tube voltages. Local servo controllers are used to achieve desired set points in these variables. It is assumed that sensors are available to measure cell current, hydrogen mole fraction in anode exhaust, and temperature of the cathode-exhaust air.

As described in the companion paper [1], the physical model represents a widely disparate range of characteristic time scales. Electrical response is essentially instantaneous (i.e., because electrochemical double-layer charging is neglected, a change in operating voltage causes an instantaneous change in current). Characteristic response times for fluid flow and diffusion are on the order of one second or less. Characteristic times for thermal response are much longer, on the order of minutes. Because of relatively fast characteristic response times and strongly nonlinear behavior, controlling electrical and exhaust characteristics is more challenging than controlling the thermal behavior. The MPC approach is particularly well suited to controlling the cell voltage and fuel flow rate. Because of the slower thermal characteristic times, a more traditional proportional-integral-derivative (PID) controller is sufficient for temperature regulation.

2.1. BOP components

Although the uncontrolled dynamics of the BOP components may be non-trival, because the BOP components are under servo control, the relevant closed loop dynamics (that is, the dynamics from a set-point to a physical variable, such as air flow) can be simplified from the point of view of the stack controller. Specifically, it is assumed that the closed loop dynamics can be approximated as linear dynamical systems with first-order lag dynamics and unity DC gain. For example, the fuel-flow subsystem is modeled as:

$$q_d = \tau_{fuel}\dot{q}_{in} + q_{in}, \quad (1)$$

where q_d is the desired fuel flow rate, τ_{fuel} is the time constant associated with the fuel-flow subsystem, and q_{in} is the fuel flow rate command that is supplied to the BOP. Analogous first-order dynamics are considered for the air-flow subsystem. Because the dynamics of the cell-voltage subsystem are very fast, it can be represented simply as a unit gain. The BOP control is not discussed further in the present paper.

3. Stack modeling

This paper concentrates primarily on the SOFC stack dynamics, which is more complicated than the BOP dynamics. The SOFC stack physical model is discussed in the companion paper [1]. The examples that follow in the present paper are based upon a particular tubular stack configuration. The tubes are 15 cm long with an outside diameter of 1 cm, which is typical of tubes that may be used in sub-kilowatt APUs. A table of model parameters that describe physical and electrochemical characteristics may be found in the

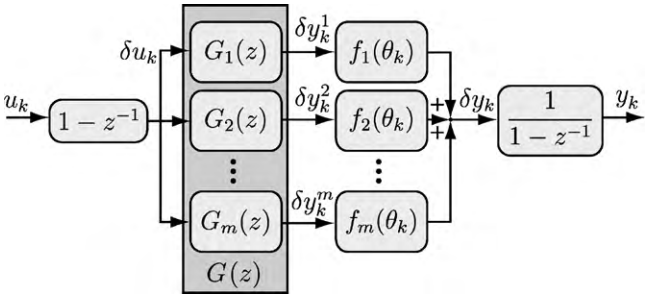

Fig. 4. LPV model structure for low-order representation.

companion paper [1]. For purposes of illustrating the model, the post-reformer SOFC inlet fuel composition is assumed to be 38% H_2, 3% H_2O, 1% CH_4, 19% CO, 0.3% CO_2, and 38% N_2. This is the equilibrium mixture that results from the partial oxidation of methane and air at 800 °C with a stoichiometric ratio to partial oxidation (i.e., oxygen to carbon ratio of 0.5), to which a small amount of steam is added to bring the steam composition to 3%. The steam is added to prevent carbon deposition in the fuel cell stack. Fuel enters the tube at 800 °C and atmospheric pressure. The cathode air, which flows around the outsides of the tubes, enters the stack at 550 °C. Both ends of the tubes conduct heat to the manifolds at a fixed temperature of 800 °C.

A typical stack can consist of 50–100 tubes, usually connected electrically in series, which is the case here. The modeling assumes an ideal stack in which all tubes behave exactly alike. Thus, net stack power and flow rates are determined from a single tube simply by multiplying the results of the single-tube model. The series connection implies that the current through all tubes is the same, while the stack voltage is the sum of the voltage across each tube. In actual operation, the system deviates from this ideal stack behavior, as the tubes are exposed to slightly different conditions. However, the idealized model is still valuable for control, as it represents the behavior of an "average" tube in the stack.

The process for obtaining the reduced-order model is twofold. First, a set of OPs is selected and locally linear models at each OP are identified to model small-signal behavior. The linear models are then combined, with redundant modes being eliminated via linear model reduction. In the second step, nonlinear functions are identified that modulate the outputs of the small-signal models in a manner similar to gain scheduling. The nonlinear functions depend upon a scheduling parameter that is assumed to be measurable (e.g., cell current).

Fig. 4 illustrates the LPV model structure, where u_k and y_k are the input and output at sampling interval k, and z is the forward shift operator. The locally linear systems, $G_i(z)$, capture the small-signal behavior at m different OPs. The system $G(z)$ represents the combined model after eliminating any redundant modes shared between the m different linear models. The variable θ is a scheduling parameter that is a function of the (measured) system output, and $f_i(\theta)$ represent gains that are nonlinear functions of θ. Because each of the linear models captures only small-signal behavior, the OP needs to be removed at the input, and added back at the output. A so-called *velocity implementation* accomplishes this by applying a first difference $(1 - z^{-1})$ of the input, and integrating $(1 - z^{-1})^{-1}$ the output.

3.1. OP selection

For expected ranges of stack operation, it is desired to pick a few OPs whose dynamics can be used to span the the entire operating space. To select such points, a series of steady-state simulations

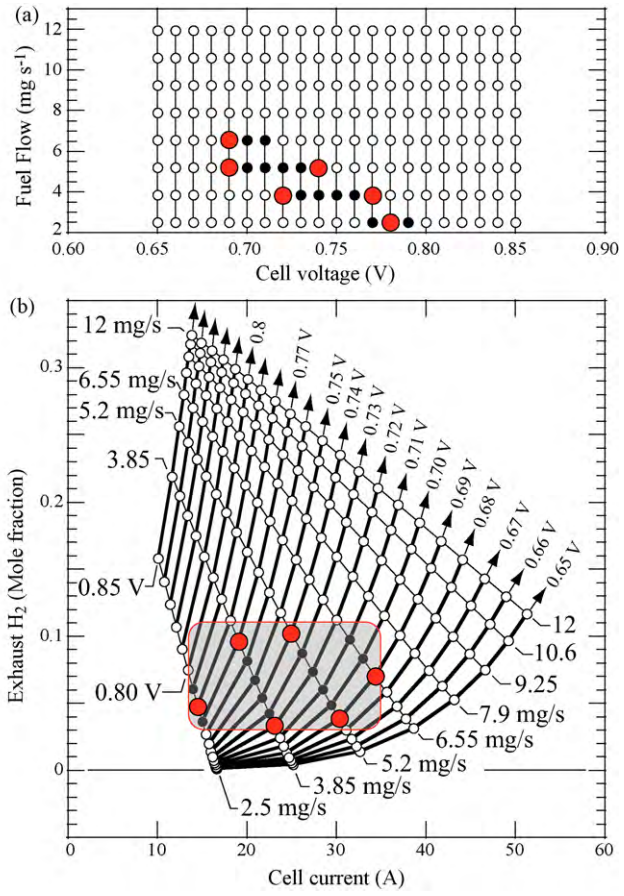

Fig. 5. Input–output map from steady-state simulation. (a) Steady-state input map. (b) Steady-state output map.

with different input values are recorded. Fig. 5 illustrates an input map and the resulting output map. In these simulations, cell voltage ranges from 0.65 V to 0.85 V in steps of 0.01 V. At each cell voltage, fuel flow changes between 2.5 mg s^{-1} (velocity = 0.247 m s^{-1}) and 12 mg s^{-1} (velocity = 1.19 m s^{-1}). The corresponding steady-state outputs define a region in which, roughly speaking, cell current changes between 10 A (per tube) to 55 A (per tube) and H_2 concentration in exhaust varies from 0 to 35%.

The practical operating space should be more restricted than the potential operating space shown in Fig. 5. To achieve high efficiency and to minimize cell damage, the cell voltage should be limited as $0.67 \leq E_{cell} \leq 0.79$. Because of a need for fuel into the tail-gas combustor for cathode-air preheating (Fig. 1) and to limit deleterious reoxidation of the SOFC anode, fuel utilization should be in the range of 70–90%. In the present simulations, this limitation corresponds to maintaining hydrogen in the anode exhaust as $3\% < X_{H_2} < 11\%$. The combination of these considerations limit the cell current (per tube) as $13\,A < I_{cell} < 35\,A$.

The practical limitations in the steady-state output space are illustrated in Fig. 5b as a shaded rectangle. Six OPs are selected (shown as large red dots) along the output boundaries to represent the operating space. The selected output space is mapped back to the input space with corresponding markers in Fig. 5a. The selected OPs along with their corresponding output values are also listed in Table 1(a) and (b), respectively. In the following sections, a linear dynamic model is identified at each operating point, and scheduling functions are identified that blend the linearized dynamics between operating points.

Table 1
Selected OPs data.

OP num.	Cell voltage (V)	Fuel flow ($mg\,s^{-1}$)
(a) Input data		
1	0.78	2.5
2	0.77	3.85
3	0.72	3.85
4	0.74	5.20
5	0.69	5.20
6	0.69	6.55
OP num.	**Cell current (A)**	**H_2 (mole fraction)**
(b) Output data		
1	14.51	0.047
2	19.07	0.096
3	23.10	0.032
4	24.96	0.102
5	30.31	0.038
6	34.31	0.070

3.1.1. Identification of linear models

At each OP in Table 1(a), a linear dynamic model is identified that captures the dominant small-signal dynamics at that point. This can be accomplished using linearization followed by model reduction. However, the present approach uses the data-based model reduction method discussed in the companion paper [1]. The data-based identification is accomplished with a series of straightforward simulations, and is essentially independent of complexity in the underpinning physical model. Transient simulations in which the input variables are systematically perturbed provides the data from which the reduced-order is obtained. The input variables are cell voltage, fuel mass flow rate, and air mass flow rate. The output variables are cell current, hydrogen mole fraction in anode exhaust, and cathode-exhaust air temperature. The sampling time of the perturbations is $T_s = 0.125$ s, which is also the sampling time of the controller that is being designed. To take advantage of possible repeated modes between different OPs, the small-signal models are assembled into a single model, as illustrated in Fig. 6. Thus, the output of the identified system may be written as $\delta y = [\delta y^1\ \delta y^2 \cdots \delta y^m]$ where δy^i is the small-signal response of the system at OP_i.

3.2. Identification of scheduling functions

Using the results of the previous section, the small-signal models, $G_i(z)$ ($i = 1, 2, \ldots, m$), are available for $m = 6$ different OPs. In other words, each $G_i(z)$ captures the small-signal behavior for one value of the scheduling parameter, θ. A set of scheduling functions $f_i(\theta)$ ($i = 1, 2, \ldots, m$) is needed to match the overall system response to large-signal variations. As shown in Fig. 4, the functions $f_i(\theta)$ are weighting factors that combine the outputs of the linearized models. This means that $f_i(\theta)$ describes how closely model i describes the model dynamics at scheduling point θ, and thus can be thought of as a correlation metric between the current operating condition and operating point i.

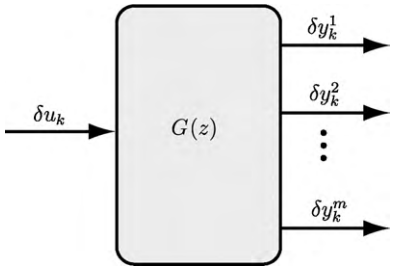

Fig. 6. Combined linear model at multiple OPs.

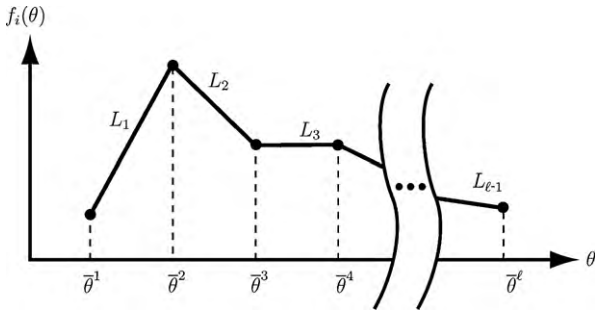

Fig. 7. A postulated scheduling function $f_i(\theta)$.

As an alternative to developing a parameterized basis expansion of $f_i(\theta)$, estimates of $f_i(\theta)$ can be found directly in terms of the function values. Specifically, the scheduling parameter θ is quantized into a fixed number of "bins" with centers $\bar{\theta}^j$ ($j = 1, 2, \ldots, \ell$), with the objective being to estimate the values for $f_i(\bar{\theta}^j)$ for all i, j as illustrated schematically in Fig. 7. In other words, the set of values $f_i(\bar{\theta}^j)$ for all i, j are parameters to be identified. Note that ℓ can be much larger than m. Once the values of $f_i(\bar{\theta}^j)$ are found, the functions $f_i(\theta)$ can be represented by an appropriate interpolation. Given a measured scheduling sequence θ_k, the quantized scheduling sequence $\bar{\theta}_k$ is established such that for all k, $\bar{\theta}_k = \bar{\theta}^j$ for some j, and the Euclidean norm $\|\theta_k - \bar{\theta}_k\|$ is minimized.

Because the small-signal models $G_i(z)$ are known for $i = 1, 2, \ldots, m$, the signals

$$\delta y_k^i = G_i(z)(1 - z^{-1})u_k \tag{2}$$

can be calculated, where u_k are the actuation inputs used in the simulations. The simulation outputs y_k and quantized scheduling sequence $\bar{\theta}_k$ are also known. The objective is to select values of $f_i(\bar{\theta}^j)$ such that $\delta y_k \approx \delta \hat{y}_k$, where δy_k is the first difference of the measured output

$$\delta y_k = (1 - z^{-1})y_k, \tag{3}$$

and

$$\delta \hat{y}_k = \sum_{i=1}^{m} f_i(\bar{\theta}_k)\delta y_k^i. \tag{4}$$

In other words, the objective is to find

$$\underset{f_i(\bar{\theta}^j)}{\operatorname{argmin}} \sum_{k=1}^{N} \|\delta y_k - \delta \hat{y}_k\|^2, \tag{5}$$

so that the scheduling functions blend the small-signal models to best match the observed output. However, without placing restrictions on $f_i(\bar{\theta}^j)$, the minimization problem is under-determined, meaning that many different functions can make the objective function equal zero. Thus, constraints are required. The imposed constraints are natural choices. One set of constraints come from the definition of the scheduling functions: they must range between 0 and 1 ($0 \le f_i(\bar{\theta}^j) \le 1$), and the sum of the scheduling functions over i for any $\bar{\theta}^j$ must always be unity ($\sum_{i=1}^{m} f_i(\bar{\theta}^j) = 1$). Moreover, the value of each scheduling function at its corresponding OP should be equal to unity, i.e. $f_i(\bar{\theta}^j = \phi^i) = 1$, where ϕ^i is the value of $\bar{\theta}^j$ that corresponds to the OP for system $G_i(z)$. However, the optimization problem is still under-determined. Including a regularization term in the objective function solves the problem. This term makes the identified functions sufficiently smooth. As introduced by Hsu et al. [19], a *dispersion function* is used as a measure of smoothness for the non-parametric identification of nonlinear systems. The dispersion function is a smoothness measure for functions that are described point-wise, and is closely related to total

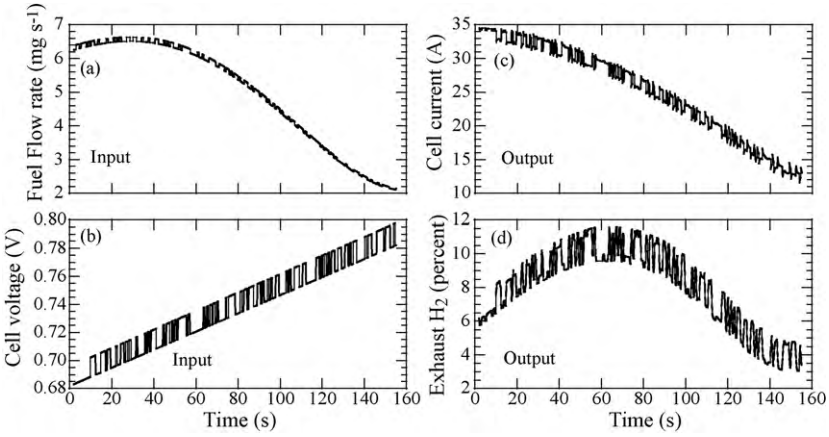

Fig. 8. Large-signal variation simulation.

variation. It can also be extended to multi-dimensional functions, but for simplicity it is restricted here to scalar $\bar{\theta}$. Given a point-wise description of a function in terms of points $(\bar{\theta}^j, f(\bar{\theta}^j))$, the dispersion of f is defined as

$$\Psi(f(\bar{\theta}^j)) = \sum_{j=1}^{\ell-1} L_j^2, \tag{6}$$

where L_j are the lengths of a linear interplant of $(\bar{\theta}^j, f(\bar{\theta}^j))$ (Fig. 7). The dispersion is a quadratic function of the values of $f_i(\bar{\theta}^j)$. Adding the constraints and adding the smoothness measure to the objective function, the optimization problem can be written as

$$\begin{aligned} \min_{f_i(\bar{\theta}^j)} \quad & \sum_{k=1}^{N} \|\delta y_k - \delta \hat{y}_k\|^2 + \beta \sum_{i=1}^{m} \Psi(f_i(\bar{\theta}^j)) \\ \text{subject to} \quad & 0 \le f_i(\bar{\theta}^j) \le 1, \\ & \sum_{i=1}^{m} f_i(\bar{\theta}^j) = 1, \\ & f_i(\phi^i) = 1, \end{aligned} \tag{7}$$

where β is a user-defined parameter that can be varied to affect the smoothness of the scheduling functions. Because the dispersion is a quadratic function of $f_i(\bar{\theta}^j)$, Eq. (7) is a convex optimization problem that can be easily solved using modern optimization packages as a second order cone problem. The results in this paper for implementing the LPV algorithm were obtained using CVX [20,21] toolbox in the computational software Matlab. By solving the optimization problem, the values of the scheduling functions $f_i(\bar{\theta}^j)$ are calculated for all i, j that minimize a weighted sum of the fit error and the dispersion, subject to the constraints.

By augmenting the linear state-space representation with the past input and output (u_{k-1} and y_{k-1}), the final result is a parameter-varying state-space model of the form

$$\begin{bmatrix} u_k \\ x_{k+1} \\ y_k \end{bmatrix} = \begin{bmatrix} 0 & 0 & 0 \\ -\Gamma & \Phi & 0 \\ -D(\theta) & C(\theta) & I \end{bmatrix} \begin{bmatrix} u_{k-1} \\ x_k \\ y_{k-1} \end{bmatrix} + \begin{bmatrix} I \\ \Gamma \\ D(\theta) \end{bmatrix} u_k, \tag{8}$$

where

$$C(\theta) = [f_1(\theta)\, f_2(\theta) \cdots f_m(\theta)]C, \tag{9}$$

$$D(\theta) = [f_1(\theta)\, f_2(\theta) \cdots f_m(\theta)]D, \tag{10}$$

and (Φ, Γ, C, D) are state-space matrices associated with the dynamics of the combined model $G(z)$.

3.2.1. LPV-based nonlinear identification

Consider an example to illustrate the use of an LPV scheme for the nonlinear system identification of the SOFC stack. Cell current is chosen as the scheduling parameter. Using other output variables, or combinations of output variables, as the scheduling variable is discussed in the following section. The stack OPs are specified by two input variables, cell voltage and fuel flow rate. To transition between different OPs, a transient simulation is designed in which the output variables vary greatly within the acceptable operating space (Fig. 5). Fig. 8a and b shows the temporal variation of the input signals fuel flow rate and cell voltage. Fig. 8c and d shows the corresponding output responses for cell current and H_2 in the anode exhaust. To assist understanding how large-signal variations move within the region defined by selected OPs, Fig. 9 illustrates the changes in input and output spaces.

By solving the optimization problem as described by Eq. (7), six scheduling functions are identified. Fig. 10 illustrates the six scheduling functions where cell current is used as the scheduling parameter. A value of $\beta = 1$ is used. As required by the constraints,

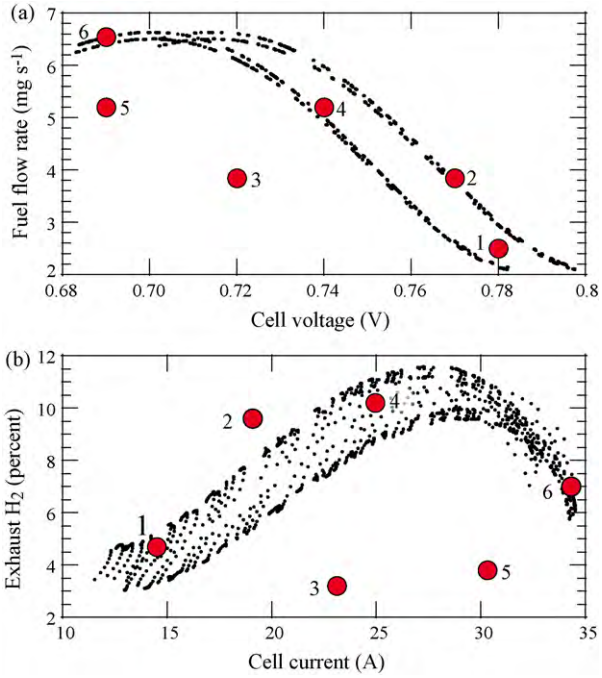

Fig. 9. Large-signal simulation. (a) Variation in input space over selected OPs. (b) Variation in output space over selected OPs.

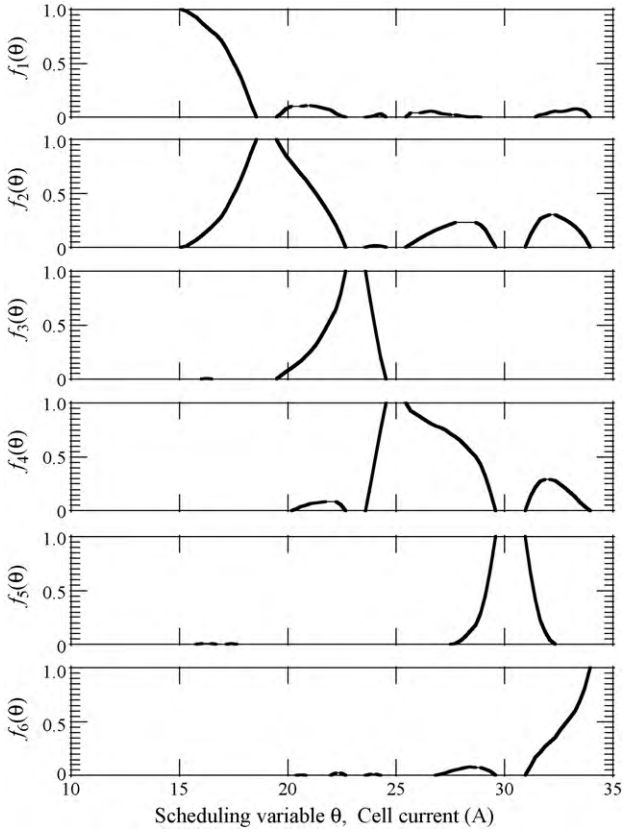

Fig. 10. Identified scheduling functions using cell current as the scheduling variable.

the function values all satisfy $0 \leq f_i(\theta) \leq 1$, and at each value of cell current $\sum_i f_i(\theta) = 1$. Because the OPs are labeled in the order of cell current (Table 1(b)), the functions have peaks in order from $f_1(\theta)$ to $f_6(\theta)$ as the output current (i.e., θ) increases. For example, because OP_2 has an output current of about 20 A, at $\theta \approx 20$ A all the functions are nearly zero except $f_2(\theta)$.

Within the LPV structure, the integrator is modified by adding a simple error-correction term (predictor) as

$$\tilde{y}_k = \tilde{y}_{k-1} + \delta\hat{y}_k + L(y_{k-1} - \tilde{y}_{k-1}), \tag{11}$$

where $\tilde{y}_k$ is the output of the LPV model, y_k is the output of the actual system (here the physical model) and $\delta\hat{y}_k$ is calculated as in Eq. (4). The objective is to reduce error accumulation in the integrator. Since the model is intended to be used for real-time control, the value of the system output y_{k-1} is available from actual sensors, or sensor inferences. In Eq. (11), the prediction parameter L is a free parameter, which can be chosen based on the length of the experiment and the output variable. A value of 0.05 is chosen in the results presented here.

The fidelity of the reduced-order models can be evaluated by direct comparison with the detailed physical model. Fig. 11 shows the results of both the low-order identified model and the full physical model, both being driven by the input transients shown in Fig. 8a and b. To within the thickness of the lines, the two models produce essentially indistinguishable results. The LPV method, based on smooth combinations of small-signal linear models, delivers an excellent representation of the nonlinear physical behavior over wide ranges of operating conditions.

3.3. Selection of scheduling variable

Although cell current was used as the LPV scheduling parameter in the previous example, it is not the only choice. Fig. 12 illustrates

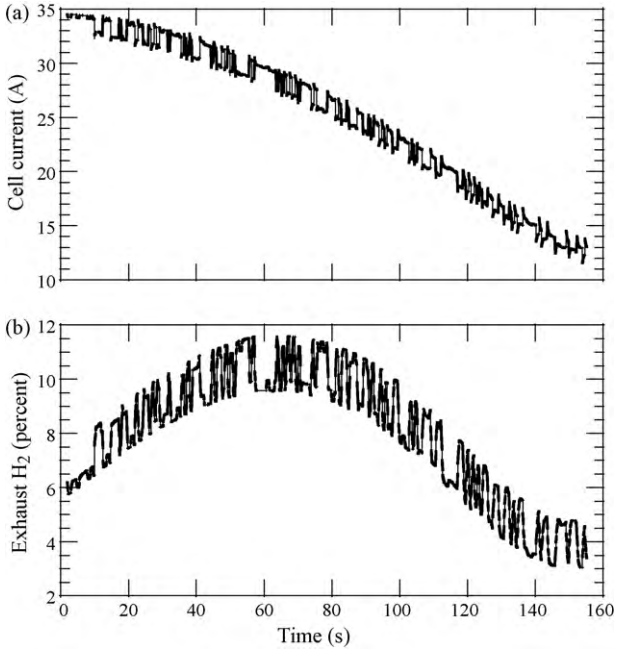

Fig. 11. Comparison between outputs from physically based high-order model and the LPV-based low-order model over a wide range of operation. The results are essentially indistinguishable.

the scheduling functions that are estimated when using hydrogen in the anode exhaust as the scheduling parameter. It is also possible to use more than one variable for scheduling. For instance, a combination of both cell current and exhaust hydrogen can be considered.

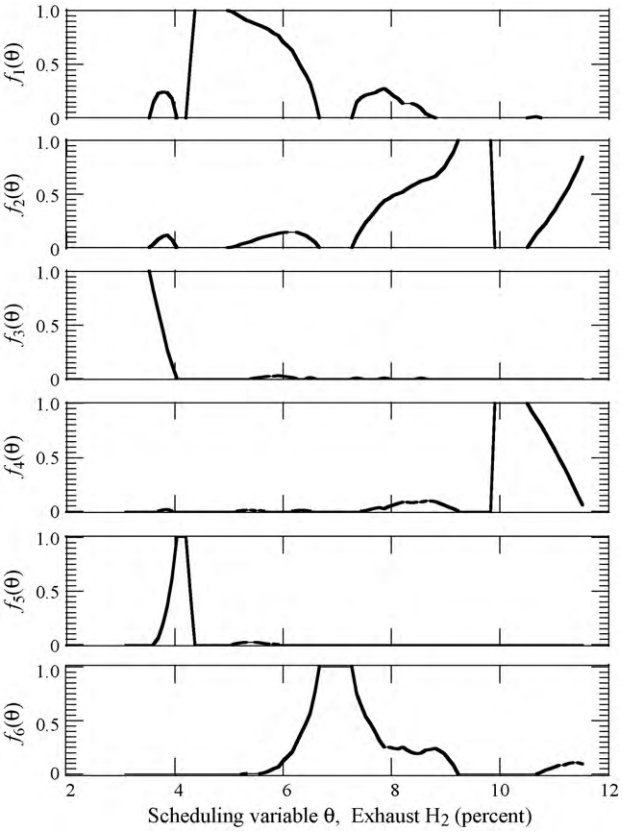

Fig. 12. Identified scheduling functions with H_2 mole fraction in anode exhaust as the scheduling variable.

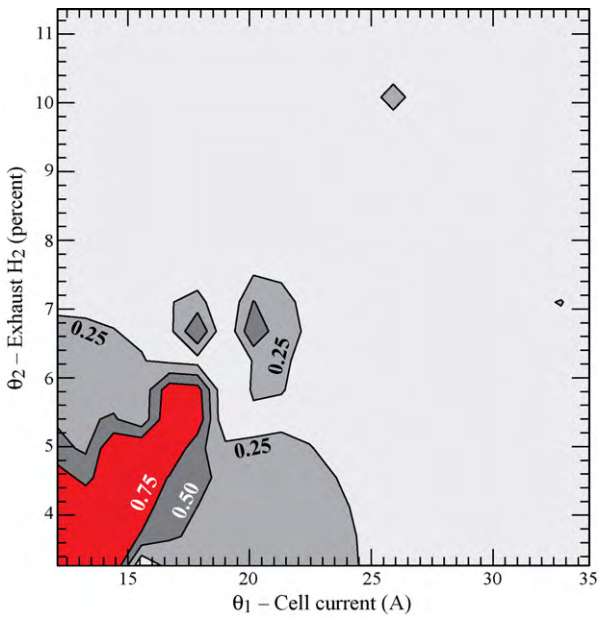

Fig. 13. Two-dimensional scheduling function as identified using cell current and exhaust H_2 as the scheduling variables at OP_1. The function $f_1(\theta_1, \theta_2) \approx 1$ is highest in the left-lower corner, which corresponds to the cell current and exhaust H_2 for OP_1.

In this case, the scheduling functions $f_i(\theta_1, \theta_2)$ are two-dimensional functions which must be identified by solving a slightly-modified optimization problem, specifically, two-dimensional dispersion functions are employed as described in [19]. Intuitively, one might expect that the extended approach would deliver a higher fidelity identification, and thus improve performance of the reduced model. Fig. 13 is a two-dimensional contour representation of $f_1(\theta_1, \theta_2)$ corresponding to OP_1 (Table 1(b)), where both cell current and exhaust hydrogen are the scheduling variables. The scheduling function is essentially unity (i.e., $f_1(\theta_1, \theta_2) \approx 1$) in the left lower corner, which corresponds to the values of cell current and exhaust H_2 around OP_1. Performance at other OPs is similar.

Based on the simulation results for the present problem, there is little, if any, benefit in using the two-dimensional scheduling. Table 2 shows the root-mean-square (RMS) error associated with the alternative scheduling approaches. It is interesting to note that scheduling based on current provides a slightly better result than scheduling with exhaust hydrogen. Based on these results, it appears that the two scheduling variables are correlated. Thus, for SOFC stack control, cell current is preferable because it is much easier to measure in practice.

4. Model predictive control

The need to maintain signal constraints during operation, combined with the importance of unmeasured variables such as internal stack temperature or fuel utilization, indicate the need for advanced control strategies. Because of these important operating considerations, as well as the strong interaction between input variables, MPC is a natural choice for control implementation. MPC provides a means to incorporate quantitative physical understanding into real-time process-control decisions. The SOFC stack is a complex nonlinear system, with widely disparate ranges of characteristic time scales. Moreover, there are multiple actuation possibilities and a variety of possible sensors. It is a challenging task to design and implement a control strategy that achieves optimal performance through the coordination of multiple sensors and actuators.

Table 2
Comparison between different scheduling approaches.

Scheduling variable	RMS error (%)
Cell current alone	0.16504
Exhaust H_2 alone	0.17632
Cell current and exhaust H_2	0.16121

The MPC design is accomplished in two distinct parts: (1) estimate the current system state from observations of past inputs u and outputs y, and (2) establish future actuation trajectories u to guide the system through a desired output trajectory.

4.1. State estimation

Assume that the process started at time $k = 0$, and the current time is $k = k_0$. The first task of an MPC controller is to use recorded sensor measurements $y_k\,(k = 0, 1, \ldots, k_0)$ to determine an estimate for the current state of the plant, x_{k_0}. Because actuation commands are also recorded over time, the input–output information $(u_k, y_k)\,(k = 0, 1, \ldots, k_0)$ is available at time k_0. At any time step k, the differences in actuation commands and output measurements can be calculated as $\delta u_k = u_k - u_{k-1}$ and $\delta y_k = y_k - y_{k-1}$, respectively. The current state x_{k_0} can be estimated by solving the following optimization problem:

$$\min_{x_k} \left(\sum_{k=0}^{k_0} \|e_k\|^2 + \sum_{k=0}^{k_0-1} \|w_k\|^2 \right), \tag{12}$$

where

$$e_k = R^e \left[\delta y_k - \left(C\left(\theta\right) x_k + D\left(\theta\right) \delta u_k \right) \right], \tag{13}$$

$$w_k = Q^e \left[x_{k+1} - \left(\Phi x_k + \Gamma \delta u_k \right) \right], \tag{14}$$

and Q^e and R^e are weighing matrices. The state-estimation process can be interpreted as follows: (1) find the state sequence $\hat{x}_k\,(k = 0, 1, \ldots, k_0)$ that minimizes a weighted combination of the error e_k between the (small-signal) measurements (sensors) and the model outputs and the adjustment term w_k, needed to match the dynamic updates, and (2) take the last element of the state sequence $\hat{x}_k$ as the current state of the plant, $\hat{x}_{k_0}$. The error (e_k, Eq. (13)) can be interpreted in the context of the reduced-order model (Eq. (8)). At each scheduling variable value θ, the sensors measure the difference in output between two successive steps as δy_k while the model predicts the difference as $C(\theta)x_k + D(\theta)\delta u_k$. The adjustment w_k is the difference between the state x_{k+1} at the next step and model-predicted state at the next step, $\Phi x_k + \Gamma \delta u_k$.

The relative weighting matrices Q^e and R^e can be chosen based upon engineering judgment, or they can be chosen based on a stochastic model for measurement errors and disturbances. In either case, state estimation is a quadratic optimization problem. If the system is observable, the minimizer is unique. In this example, Q^e and R^e are scaled identity matrices as $R^e = 0.1 I_p$ and $Q^e = I_n$ where p is the number of outputs and n is the number of states. The size of optimization problem (Eq. (12)) grows significantly as k_0 increases. Fortunately, the Kalman filter can implement the estimation process recursively [22]. That is, a gain sequence K_k can be calculated such that the output of the system,

$$\hat{x}_{k+1} = \Phi \hat{x}_k + \Gamma u_k + K_k[\delta y_k - (C(\theta)x_k + D(\theta)\delta u_k)], \tag{15}$$

produces the same sequence of estimates for $\hat{x}_k$.

4.2. Control

The role of control is to choose future actuation that guides the system according to a desired trajectory. Assume that a desired output trajectory can be specified as y_k^d for $k = k_0, \ldots, k_0 + p$. The

control is chosen to best match the desired output trajectory over a look-ahead horizon of p sampling intervals, while meeting fixed constraints on input and output excursions. At every time k_0 the current state $\hat{x}_{k_0}$ is estimated according to the foregoing optimization problem (i.e., Eq. (12)) and the system output at time k_0 is measured. After choosing weighting matrices R^c and Q^c and constraints b_{ui} and b_{yi}, the following optimization problem is solved:

$$\begin{aligned} \min_{u_k} \quad & \sum_{k=k_0}^{k_0+p} \|R^c(y_k^d - y_k)\|_1 + \|Q^c u_k\|_1 \\ \text{subject to} \quad & x_{k+1} = (\Phi x_k + \Gamma u_k) \\ & y_k = C(\theta)x_k + D(\theta)\delta u_k + y_{k-1} \\ & b_{u1} < u_k < b_{u2} \\ & b_{y1} < y_k < b_{y2} \end{aligned} \tag{16}$$

and the first element u_{k_0} of the optimal sequence u_k ($k = k_0, k_0+1, \ldots, k_0+p$) is applied as the plant input (control law) for the next time interval. In the example that follows, the horizon is chosen as $p = 12$. For a sampling interval of $T_s = 0.125$ s, the horizon is 1.5 s. Weighting matrices Q^c and R^c are square diagonal matrices with different weights for different input and output variables. In this example, $Q^c = \text{diag}([\,2.5 \times 10^7 \quad 10^3\,])$ where 2.5×10^7 is the weight on fuel flow rate and 10^3 is the weight on cell voltage, and $R^c = \text{diag}([\,30 \quad 200\,])$ where 30 is the weight on cell current and 200 is the weight on exhaust H_2.

4.3. Controller performance

To evaluate performance, an MPC controller is used to control the physical SOFC model through a specified transient trajectory of desired output current, while also satisfying constraints. The controller uses the low-order LPV-based model for state estimation and actuation sequences. Fig. 14a shows both the desired current trajectory and the achieved cell current using the MPC controller. At this scale, the two curves are nearly indistinguishable. Fig. 14b is an expanded graph over a short time interval that reveals some small differences between the desired and achieved cell-current histories. The desired current spans a significantly wide range, over which the physical behavior is strongly nonlinear. Although near step-changes in the desired current trajectory, some small overshoots are present, the MPC controller is delivering excellent performance.

In addition to achieving the desired cell-current trajectory (Fig. 14), the controller is able to respect constraints on the input and output variables. Fig. 15a and b shows the controlled input variables. In actual operation, the manipulated voltage is the sum of the voltages across each cell, but here the "average" cell voltage, or total voltage divided by number of cells, is reported. The controller maintains the commanded cell voltage and fuel flow rate within the defined bounds (shown as the dashed lines). Cathode-air inlet flow rate is also controlled. However, for the short time interval shown in Fig. 15, it is essentially unchanged. Fig. 15c and d show the output variables. The anode-exhaust hydrogen mole fraction remains in the desired pre-specified bounds. Because of long thermal time constants, the cathode-exhaust air temperature varies relatively little over the short 40 s time interval.

These results show that the MPC controller provides excellent performance over a very demanding cell-current trajectory. Moreover, the controller meets the load demand, while also respecting

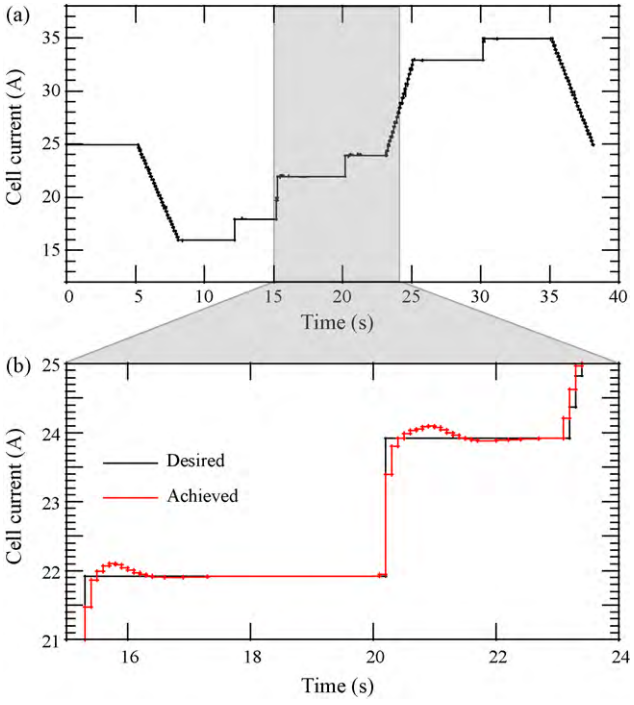

Fig. 14. (a) Comparison between the desired cell current and the cell current delivered by the MPC controller. At this scale, the controlled result is essentially within a line thickness of the desired current. (b) An expanded section of the trajectory, revealing some small differences between desired and achieved cell current.

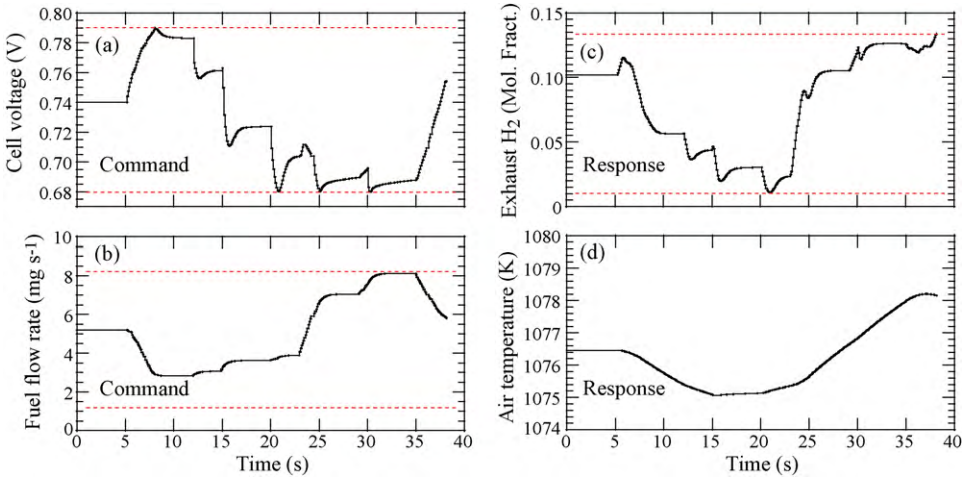

Fig. 15. MPC controlled input commands and model-predicted responses. Pre-specified bounds are shown with dashed lines. (a) Controller-commanded cell voltage. (b) Controller-commanded fuel flow rate. (c) Hydrogen mole fraction in the anode exhaust. (d) Cathode-air exhaust temperature.

constraints on input and output variables. Qualitatively, the controller is making some anticipated decisions. For example, when the load decreases at around 5 s, the cell voltage increases and the fuel flow rate decreases. As the load demand increases, the cell voltage decreases and fuel flow rate increases. However, it would be difficult, if not impossible, to achieve the complex set of controller commands with less capable control strategies such as a PID regulator. Moreover, controllers such as PID are not capable of respecting input and output constraints.

5. Summary and conclusions

A systematic approach is used to incorporate physical knowledge into the control of an SOFC stack. The process begins with a transient, high-fidelity, physical model. Such models, are too computationally expensive to be considered for direct incorporation into real-time control. Reduced-order locally linear models are required. However, the reduced models must be predictive over wide operating ranges, and thus capture nonlinear behaviors. Model reduction here is accomplished using an LPV structure. Results show that by smoothly scheduling between operating conditions, nonlinear behaviors can be adequately represented by combinations of low-order locally linear models. At certain steady-state OPs that span the expected operating space, locally linear models are identified by systematic perturbations of the high-order physical model. An MPC controller is designed and implemented based on the reduced-order models. In addition to meeting load-demand transients, the MPC controller can also be designed to satisfy constraints on actuation commands (e.g., cell voltage and fuel flow rate) and on output responses (e.g., fuel utilization). To evaluate performance, the LPV-based MPC controller is used to control the physically based high-order model. Although scheduling between low-order linear models can depend upon multiple output variables, results show that scheduling based on the cell current alone provides excellent results.

References

[1] A.M. Colclasure, B.M. Sanandaji, T.L. Vincent, R.J. Kee, Modeling and control of tubular solid-oxide fuel cell systems. I. Physical models and linear model reduction. J. Power Sources 196 (2010) 196–207.
[2] R.J. Kee, H. Zhu, D.G. Goodwin, Proc. Combust. Inst. 30 (2) (2005) 2379–2404.
[3] R.J. Kee, H. Zhu, A.M. Sukeshini, G.S. Jackson, Combust. Sci. Technol. 180 (6) (2008) 1207–1244.
[4] T.L. Vincent, B.M. Sanandaji, A.M. Colclasure, H. Zhu, R.J. Kee, ECS Trans. 25 (2009) 1175–1184.
[5] D.J. Hall, R.G. Colclaser, IEEE Trans. Energy Convers. 14 (3) (1999) 749–753.
[6] J. Padulles, G.W. Ault, J.R. McDonald, J. Power Sources 86 (1–2) (2000) 495–500.
[7] J.T. Pukrushpan, A.G. Stefanopoulou, H. Peng, Control of Fuel Cell Power Systems: Principles, Modeling, Analysis and Feedback Design, Springer Verlag, 2004.
[8] J. Yang, X. Li, H.G. Mou, L. Jian, J. Power Sources 188 (2) (2009) 475–482.
[9] J. Arriagada, P. Olausson, A. Selimovic, J. Power Sources 112 (1) (2002) 54–60.
[10] H.B. Huo, X.J. Zhu, W.Q. Hu, H.Y. Tu, J. Li, J. Yang, J. Power Sources 185 (1) (2008) 338–344.
[11] X. Wang, B. Huang, T. Chen, J. Process Control 17 (2) (2007) 103–114.
[12] J. Hasikos, H. Sarimveis, P.L. Zervas, N.C. Markatos, J. Power Sources 193 (1) (2009) 258–268.
[13] Q. Chen, L. Gao, R.A. Dougal, S. Quan, J. Power Sources 191 (2) (2009) 473–482.
[14] Q. Li, W. Chen, Y. Wang, J. Jia, M. Han, J. Power Sources 194 (1) (2009) 338–348.
[15] M.A. Danzer, J. Wilhelm, H. Aschemann, E.P. Hofer, J. Power Sources 176 (2) (2008) 515–522.
[16] J. Yang, X. Li, H.G. Mou, L. Jian, J. Power Sources 193 (2) (2009) 699–705.
[17] F. Jurado, J. Power Sources 158 (1) (2006) 245–253.
[18] B.M. Sanandaji, T.L. Vincent, A.M. Colclasure, R.J. Kee, Proceedings of the ASME Dynamic Systems and Control Conference, 2009.
[19] K. Hsu, K. Poolla, T.L. Vincent, IEEE Trans. Automatic Control 53 (11) (2008) 2497–2513.
[20] M. Grant, S. Boyd, CVX: Matlab software for disciplined convex programming, version 1.21. http://cvxr.com/cvx, April 2010.
[21] J. Löfberg, Proceedings of the CACSD Conference, Taipei, Taiwan, 2004.
[22] L. Ljung, System Identification: Theory for the User, 2nd edition, Prentice-Hall, 1999.